# Experimental Demonstration of Hyperbolic Patterns

Stanis Kolpakov,[1] Adolfo Esteban-Martín,[1,2] Fernando Silva,[1] Javier García,[1]
Kestutis Staliunas,[3] and Germán J. de Valcárcel[1]

[1]*Departament d'Òptica, Universitat de València, Dr. Moliner 50, 46100 Burjassot, Spain*
[2]*ICFO, Avenida del Canal Olímpic s/n, 08860 Castelldefels, Spain*
[3]*ICREA, Departament de Física i Enginyeria Nuclear, Universitat Politècnica de Catalunya, Colom 11, 08222 Terrassa, Barcelona, Spain*

(Received 10 June 2008; published 17 December 2008)

We give experimental evidence of hyperbolic patterns in a nonlinear optical resonator. Such transverse patterns are a new kind of 2D dissipative structures, characterized by a distribution of the active modes along hyperbolas in the transverse wave-vector domain, in contrast with the usual (elliptic) patterns where the active modes distribute along rings. The hyperbolic character is realized by manipulating diffraction inside the optical resonator with cylindrical lenses. We also investigate theoretically hyperbolic patterns in corresponding Swift-Hohenberg models.

DOI: 10.1103/PhysRevLett.101.254101 PACS numbers: 05.45.−a, 47.54.−r, 82.40.Bj

*Introduction.*—Spontaneous pattern formation is a universal behavior of out of equilibrium systems, found in fields as diverse as chemistry, biology, fluid mechanics, and nonlinear optics, among others [1]. Spontaneous patterns are characterized by an intrinsic spatial scale determined by dynamical parameters (e.g., the resonator detuning in cavity nonlinear optics) and not by the geometrical constraints imposed by the boundaries [2]. The existence of a well-defined scale is related with the isotropy of the system, resulting in models of elliptic type (concerning the spatial coupling), where the nonlocality is represented by a spatial differential operator reducible to the Laplace form $\mathsf{L}_{1,1} = (\partial^2/\partial x^2 + \partial^2/\partial y^2)$ (maybe after rotation and rescaling). Such spatial coupling corresponds to, e.g., diffusion in chemistry or diffraction in optics.

Recently, pattern formation of a different, hyperbolic type has been proposed [3] for systems governed by the d'Alambert-type operator $\mathsf{L}_{1,-1} = (\partial^2/\partial x^2 - \partial^2/\partial y^2)$. Optical resonators offer such a possibility as diffraction can be manipulated, making it different along two different transverse directions. Two proposals of realization of hyperbolic systems were analyzed in Ref. [3]: (i) the use of photonic-crystal-like resonators (those with periodic modulation of the refractive index along one transverse direction [4,5]) and (ii) the use of nearly self-imaging [6–8], astigmatic resonators, as we do here: The sign of the diffraction coefficient of an optical resonator can be tuned by varying the cavity length around the self-imaging configuration, while for astigmatic resonators (with cylindrical lenses) diffraction can be manipulated separately along two orthogonal transverse directions. Self-imaging resonators have been central for the success of many nonlinear optical patterns experiments [9–11].

In this Letter, we report the first experimental observation of hyperbolic patterns. We consider both the case of a complex system (exhibiting phase invariance) and that of a real one (exhibiting bistable phase locking), which are two basic types of nonlinear optical cavities. In Ref. [3], hyperbolic patterns in a complex Swift-Hohenberg (SH) equation were numerically demonstrated. Here we analyze the real SH equation as well. Both models have been shown to rule pattern formation in a variety of nonlinear optical resonators [12–15], in particular, photorefractive oscillators [9,10], which is the system we have studied experimentally. As we are dealing with hyperbolic systems, the usual operator $\mathsf{L}_{1,1}$ appearing in SH models is replaced by $\mathsf{L}_{1,-1}$, as in [3].

*The experimental setup.*—A linear cavity photorefractive oscillator (PRO) similar to those in Refs. [9,11] (Fig. 1) was considered. The nonlinear material (a $BaTiO_3$ crystal) is pumped by two counterpropagating coherent beams coming from a single-mode 514 nm $Ar^+$ laser delivering powers around 150 mW. Refractive index gratings excited in the photorefractive crystal by the interference between the pump and the generated fields (which oscillate inside the cavity) produce a self-consistent scattering of pump energy towards the signal beams and vice versa.

The system described above is highly versatile. When one of the pump beams is blocked, nondegenerate four-wave mixing (ND4WM) occurs, leading to a complex order parameter system (similar to a laser from the nonlinear dynamics viewpoint). On the contrary, when the two pump beams act and their intensities are well balanced, the system works under degenerate four-wave mixing (D4WM), leading to a real order parameter system (behaving similarly to a degenerate optical parametric oscillator).

*The hyperbolic resonator.*—As for diffraction, lenses L1 and L2, on one hand, and L3 and L4, on the other hand (Fig. 1), form two telescopes that image the planar mirrors M and PM, respectively, close to the crystal, thus leading to a nearly self-imaging planar resonator with a very large Fresnel number. The cylindrical lens CL, having optical power along direction $y$ for definiteness, is placed at the

 

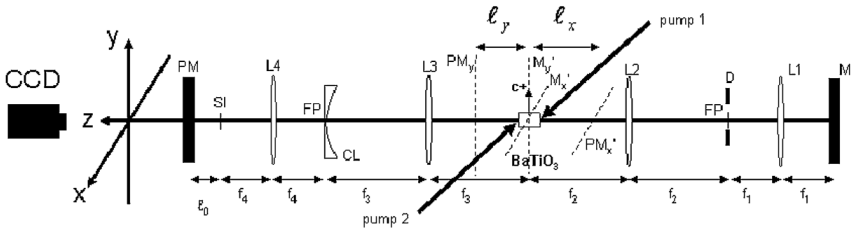


FIG. 1. Scheme of the experimental setup. M (cavity mirror), L1–L4 (lenses), CL (cylindrical lens), PM (movable piezomirror), $l_0$ (shift of the output mirror from self-imaging, SI). PM$'$ and M$'$ are the image planes of PM and M, respectively, through the corresponding set of lenses. $l_y$ and $l_x$ are effective cavity lengths; D is the mask located in the Fourier plane (FP) so as to filter transverse modes corresponding to other longitudinal modes.

Fourier plane of the left telescope, which now has two different axial magnifications corresponding to the two orthogonal transverse directions ($x$ and $y$). As a consequence, two different, effective cavity lengths (determining the diffraction coefficients [11]) occur corresponding to the two orthogonal transverse directions ($x$ and $y$): If $\ell_0$ is the shift of the output mirror (PM) from perfect self-imaging along the $x$ direction, then the effective cavity lengths through the set of lenses are given by $\ell_x = -(f_3/f_4)^2\ell_0$ and $\ell_y = \ell_x - f_3^2/f_c$, with $f_3 = 20$ cm, $f_4 = 10$ cm, and $f_c = -100$ cm the focal lengths of lenses L3, L4, and CL, respectively. In particular, hyperbolic modes are obtained when $\ell_x$ and $\ell_y$ have opposite signs. Typical effective cavity lengths used in the experiments were $\ell_x = -\ell_y = 2$ cm, achieved by shifting the output mirror by $\ell_0 = -0.5$ cm (other lengths were used as well). Note that when CL is removed (equivalently, $f_c = \infty$), $\ell_y = \ell_x$ and the resonator becomes elliptical (with perfect cylindrical symmetry around the cavity axis).

In Fig. 2, the far field emitted by the resonator is shown. Note that the pattern is similar to the transmission of the resonator under diffuse illumination. Each hyperbola (two branches each) corresponds to a cavity longitudinal mode. By varying the cavity length by means of the piezomirror PM, the detuning of each longitudinal mode (difference between the frequency of the pump and that of the mode) can be modified.

The observed far-field distribution cannot be considered in the single-longitudinal mode theoretical analysis of Ref. [3], which leads to a single hyperbola in the far field. In order to approach the theoretical treatment, we modified the experiment by filtering the far field with suitable masks in order to allow the existence of only one hyperbola (one longitudinal hyperbolic mode), so that Ref. [3] and related models can be tested experimentally.

*Modeling the hyperbolic interferometer.*—We first describe mathematically the plane-mirror resonator of Fig. 1 without the nonlinear crystal (the hyperbolic interferometer). For that we note that, at any time $t$, the field transverse distribution $A(x, y; t)$ at some reference plane is given by

$$A(x, y; t) = \mathbf{R}A(x, y; t - t_c) + \sqrt{T_{\text{in}}}\mathsf{A}_{\text{in}}(x, y; t), \tag{1a}$$

where $t_c = L/c$ is the cavity round-trip time ($c$ is the speed of light and $L$ is the total optical length in one cavity round-trip seen by the axial optical ray), $\mathsf{A}_{\text{in}}(x, y; t)$ is the amplitude of a (possibly existing) injected field, $T_{\text{in}}$ is a transmission factor,

$$\mathbf{R} = \sqrt{1 - T}\exp(ik_0L)\exp(i\mathcal{L}), \tag{1b}$$

$$\mathcal{L} = (2k_0)^{-1}(l_x\partial_x^2 + l_y\partial_y^2), \tag{1c}$$

$T$ is the fraction of energy lost (e.g., via mirror transmission) along one round-trip, $k_0$ is the light wave number, and $\mathcal{L}$ describes diffraction (coming from the integration of the paraxial Helmholtz equation). When $\text{sgn}\ell_x = \text{sgn}\ell_y$, $\mathcal{L}$ is elliptic, while if $\text{sgn}\ell_x = -\text{sgn}\ell_y$, $\mathcal{L}$ is hyperbolic. In the following, we assume, without loss of generality, $\ell_x = l > 0$ and $\ell_y = \sigma l$, where $\sigma = 1$ in the elliptic case and $\sigma = -1$ in the hyperbolic one. Upon approximating $A(x, y; t - t_c)$ by $A(x, y; t) - t_c\partial_t A(x, y; t)$, Eq. (1a) becomes $t_c\partial A/\partial t = (\mathbf{R} - 1)A + \sqrt{T_{\text{in}}}\mathsf{A}_{\text{in}}$. We assume, as usual, that $0 < T \ll 1$ and that $k_0L\,\text{mod}2\pi$ is of order $T$ (near resonance operation: $T$ sets the cavity linewidth). Both conditions render $\mathcal{L}$ small (mod$2\pi$), as we will see. Then $\mathbf{R} - 1 \approx -\frac{1}{2}T + i\sin(k_0L + \mathcal{L})$ to the leading order, where $\cos(k_0L + \mathcal{L})$ has been consistently approxi-

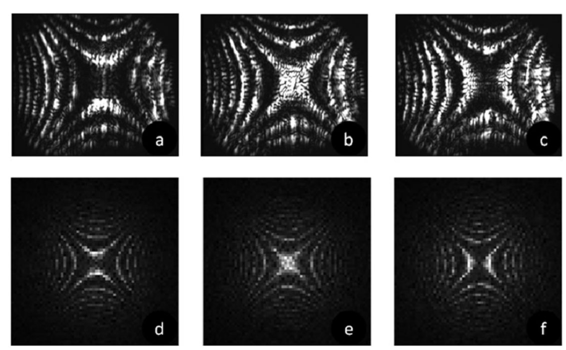


FIG. 2. Emission (far field) of the hyperbolic resonator. Experimental recordings (upper row) for (a) positive detuning, (b) zero detuning, and (c) negative detuning. The far field calculated numerically from Eq. (2) by using the speckle field for $A_{\text{in}}$ (bottom row) for (d) positive $\theta = 1$, (e) zero $\theta = 0$, and (f) negative $\theta = -1$ detuning. Parameters: $\ell_x = -\ell_y = 2$ cm, $T = 0.2$, the width of the window $\Delta k_x = \Delta k_y = 20$ cm$^{-1}$, and the width of the input far field $k_{x,0} = k_{y,0} = 10$ cm$^{-1}$.

mated by 1, and one gets finally

$$\kappa^{-1}\frac{\partial A}{\partial t} = -A + i\frac{2}{T}\sin\left[\frac{T}{2}(l_D^2 \mathsf{L}_{1,\sigma} - \theta)\right]A + A_{\rm in}, \quad (2)$$

$\kappa = cT/2L$ is the cavity linewidth, $\mathsf{L}_{1,\sigma} = \partial_x^2 + \sigma\partial_y^2$, $l_D = \sqrt{l/k_0 T}$ is a diffraction length ($l_D \sim 100\ \mu$m in our experiment), $\theta = (2/T)(-k_0 L \mathrm{mod} 2\pi) = (\omega_c - \omega_0)/\kappa$ is the cavity mistuning, with $\omega_0 = ck_0$ the radiation frequency and $\omega_c$ the closest cavity longitudinal mode frequency, and $A_{\rm in} = 2(\sqrt{T_{\rm in}}/T)\mathsf{A}_{\rm in}$. The steady solution of (2) is easily expressed in the far field [the spatial Fourier transform in terms of the transverse wave vector $(k_x, k_y)$] as $\tilde{A}(k_x, k_y) = \mathsf{T}(k_x, k_y)\tilde{A}_{\rm in}(k_x, k_y)$, where

$$\mathsf{T}(k_x, k_y) = [1 + 2iT^{-1}\sin\phi(k_x, k_y)]^{-1} \quad (3)$$

is the transmittance of the interferometer, and $\phi(k_x, k_y) = (T/2)[l_D^2(k_x^2 + \sigma k_y^2) + \theta]$. The transmission factor $|\mathsf{T}|^2$ is maximum, $|\mathsf{T}|^2 = 1$, for $\phi = 2\,m\pi$, $m$ integer, which defines the usual family of concentric rings when $\sigma = 1$, or a family of hyperbolas for $\sigma = -1$ (Fig. 3). Note that departures from that maximum as small as $\phi(k_x, k_y) = 2m\pi \pm 2T$ (recall that $0 < T \ll 1$) yield $|\mathsf{T}|^2 = 0.06$. Hence the approximation $\cos(k_0 L + \mathcal{L}) \approx 1$ we did in arriving to Eq. (2) is sensible.

Model (2) describes the multilongitudinal dynamics of the interferometer. The single-longitudinal model follows from approximating $\sin\phi \approx \phi$,

$$\kappa^{-1}\partial A/\partial t = -(1 + i\theta)A + il_D^2 \mathsf{L}_{1,\sigma}A + A_{\rm in}, \quad (5)$$

which reproduces the inner hyperbola in Fig. 2. In the following, we shall ignore the term $A_{\rm in}$ as we are not considering optical injection in our experiment.

We have considered both single-longitudinal as well as multilongitudinal mode patterns in experiments and in numerics. Here we restrict to the single-longitudinal case as the multilongitudinal mode one does not offer qualitatively new phenomena.

*Hyperbolic Swift-Hohenberg models.*—After the previous characterization of the passive resonator, it is clear that appropriate hyperbolic SH models are obtained by simply substituting the Laplacian operator $\mathsf{L}_{1,1}$ of usual SH models by $\mathsf{L}_{1,\sigma}$ [16]. As commented we shall consider the two following models:

$$\partial A/\partial t = rA - A^3 - (\mathsf{L}_{1,\sigma} - \theta)^2 A, \quad (6)$$

$$\partial A/\partial t = rA - |A|^2 A + i(\mathsf{L}_{1,\sigma} - \theta)A - (\mathsf{L}_{1,\sigma} - \theta)^2 A, \quad (7)$$

where $r$ measures the gain excess relative to threshold, which occurs at $r = 0$. In both models, all quantities are dimensionless by properly normalizing the order parameter $A$, time, and space (the latter to $l_D$). Equation (6) is a real SH model holding the symmetry $A \to -A$ and hence is appropriate for describing degenerate wave mixing [9,13]. Equation (7), already studied in the single-longitudinal mode limit in [3], is a complex SH model holding the symmetry $A \to A\exp(i\varphi)$, $\varphi$ arbitrary and hence is good for describing nondegenerate wave mixing [10]. Incidentally, we note that our analysis of the passive resonator shows that multilongitudinal models, in particular, of the SH type, can be written down directly just by substituting the differential operator of the SH model$(\mathsf{L}_{1,\sigma} - \theta)$ by $(2/T)\sin[(T/2)(\mathsf{L}_{1,\sigma} - \theta)]$ [16].

*The nondegenerate case.*—When one of the pump beams is blocked, ND4WM occurs and the PRO behaves substantially like a laser. The common patterns appearing in this case are vortices, which are phase singularities: The field intensity goes to zero at the vortex center, and the field phase goes through $2\pi$ by circulating around the vortex. Specific to the hyperbolic case is that vortices can be elongated and have a tendency to be aligned along some directions, determined by those of the hyperbola asymptotes. Depending on the character of the underlying tilted wave, two types of vortex patterns exist: If the tilted wave points to the basis of hyperbola, then the positive and negative vortices are symmetrically stretched along the different directions [Fig. 3(a)]. If the tilted wave points to one of two asymptotes of hyperbola, then the asymmetric situation is realized where the vortices of one sign are stronger stretched and of the other are almost cylindric [Fig. 3(b)]. These cases are discussed in detail in [3]. Experimental evidence of the differently stretched vortices and also of cylindric ones is given in Figs. 3(c) and 3(e), where also the angular variation of the field phase arg($A$) around two vortices (one hyperbolic, one cylindric) is shown to be affected by hyperbolicity. Good correspondence with numerically obtained vortices of the complex SH model (7) is appreciated. We note that the single-longitudinal mode operation is forced in the experiment by using suitable diaphragms located in a Fourier plane [11], which in our case are designed just to transmit light corresponding to the inner hyperbola in the far field.

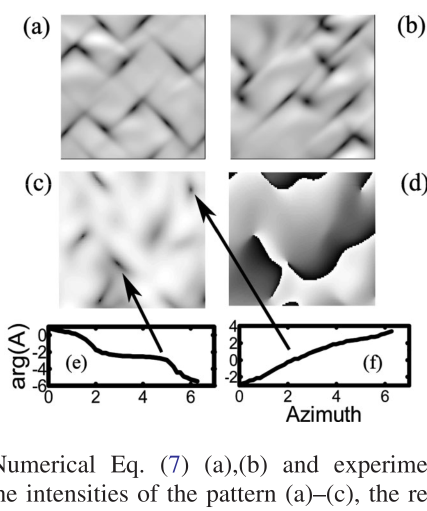


FIG. 3. Numerical Eq. (7) (a),(b) and experimental (c),(d) vortices: the intensities of the pattern (a)–(c), the reconstructed phase of the experimental pattern (d), and the variation of the field phase around the hyperbolic (e) and circular vortices (f), respectively (experiment). Parameters in numerical integration: $r = 1$, $\theta = 0.5$, window size $X = Y = 30$, integration grid $(128 \times 128)$, and integration time $t = 200$.

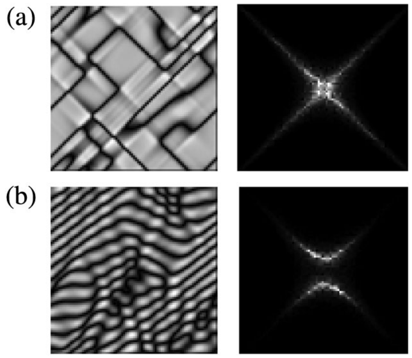

FIG. 4. Numerical patterns of the real SH Eq. (6). Left: Near-field intensity. Right: Far-field intensity. Parameters: $r = 1$, window size $X = Y = 30$, integration grid ($128 \times 128$), and (a) $\theta = 0$ and (b) $\theta = 1$. Integration time is $t = 200$.

*The degenerate case.*—By unblocking the second pump beam, D4WM occurs. Common patterns appearing in this case are rolls and phase domains [9,11].

Examples of calculated field profiles in the single-longitudinal hyperbolic SH model (6) are presented in Fig. 4, which shows saturated (quasi-steady-state) patterns. They are quasi-steady-state because usually they still display slow spatial variations. A large variety of patterns is observed, although two different regimes can be identified roughly: (i) For ''large'' detuning $|\theta| \geq 1$, patterns are usually rolls, comprised of two spots in the far field residing on the resonant hyperbola. Sometimes two rolls appear (two pairs of spots in the far field) resulting in two domains of differently oriented rolls. (ii) For ''small'' detuning $|\theta| < 1$, when the hyperbola degenerates into a cross (see Fig. 2), phase domains are observed. The domain boundaries are oriented along the axes of the hyperbola, i.e., $|x| = |y|$. Curiously, in this case the domain boundaries form a broken structure at angles between domains around 90°.

Finally, in Fig. 5, we show examples of experimentally recorded hyperbolic patterns for different detunings. The hyperbolic character is evidenced in the near-field pattern by the different slopes and different spatial frequencies observed, as well in the far field.

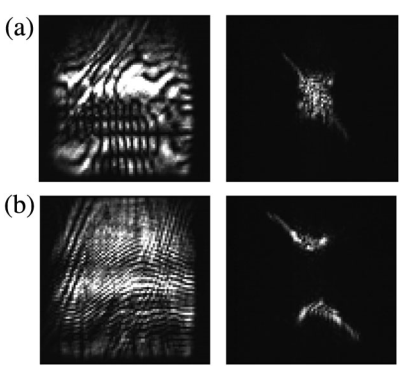

FIG. 5. Experimental recordings of the near (left column) and far field (right column) of hyperbolic patterns depending on detuning when only one longitudinal mode is allowed by spatial filtering. (a) Phase domains close to zero detuning. (b) Rolls with different orientations and spatial scales for large detuning.

In conclusion, we have given evidence of hyperbolic transverse patterns (vortices, rolls, and phase domains) in a nonlinear optical cavity. Unlike usual (cylindric) patterns, hyperbolic ones can be composed of different spatial scales and orientations. Simulations of universal (Swift-Hohenberg) models are in qualitative agreement with the experiments.

We acknowledge discussions with E. Roldán and J.C. Soriano. The work has been supported by Projects No. FIS2005-07931-C03-01 and No. FIS2005-07931-C03-03 of Spanish Ministerio de Educación y Ciencia and European Project BRIGHTLIGHT.

[1] M. C. Cross and P. C. Hohenberg, Rev. Mod. Phys. **65**, 851 (1993); D. Walgraef, *Spatio-Temporal Pattern Formation* (Springer, New York, 1996); M. I. Rabinovich, A. B. Ezersky, and P. D. Weiman, *The Dynamics of Patterns* (World Scientific, Singapore, 2000).

[2] A. C. Newell and J. V. Moloney, *Nonlinear Optics* (Westview Press, Boulder, CO, 2003); P. Mandel, *Theoretical Problems in Cavity Nonlinear Optics* (Cambridge University Press, Cambridge, England, 1997); L. A. Lugiato, M. Brambilla, and A. Gatti, *Optical Pattern Formation*, Adv. At. Mol. Opt. Phys. Vol. 40 (Academic Press, New York, 1998), p. 229; F. T. Arecchi, S. Boccaletti, and P. L. Ramazza, Phys. Rep. **318**, 1 (1999); N. N. Rosanov, *Spatial Hysteresis and Optical Patterns* (Springer, New York, 2002); K. Staliunas and V. J. Sánchez-Morcillo, *Transverse Patterns in Nonlinear Optical Resonators* (Springer, New York, 2003).

[3] K. Staliunas and M. Tlidi, Phys. Rev. Lett. **94**, 133902 (2005).

[4] K. Staliunas, Phys. Rev. Lett. **91**, 053901 (2003); K. Staliunas, Phys. Rev. E **70**, 016602 (2004).

[5] D. Gomila, R. Zambrini, and G.-L. Oppo, Phys. Rev. Lett. **92**, 253904 (2004); D. Gomila and G.-L. Oppo, Phys. Rev. E **72**, 016614 (2005).

[6] J. A. Arnaud, Appl. Opt. **8**, 189 (1969).

[7] V. Yu. Bazhenov, V. B. Taranenko, and M. V. Vasnetsov, Proc. SPIE Int. Soc. Opt. Eng. **1806**, 14 (1993).

[8] M. Saffman, D. Montgomery, and D. Z. Anderson, Opt. Lett. **19**, 518 (1994).

[9] V. B. Taranenko, K. Staliunas, and C. O. Weiss, Phys. Rev. Lett. **81**, 2236 (1998).

[10] A. Esteban-Martín *et al.*, Phys. Rev. Lett. **97**, 093903 (2006).

[11] A. Esteban-Martín *et al.*, Phys. Rev. A **69**, 033816 (2004) Opt. Express **13**, 3631 (2005).

[12] J. Lega, J. V. Moloney, and A. C. Newell, Phys. Rev. Lett. **73**, 2978 (1994); K. Staliunas, Phys. Rev. A **48**, 1573 (1993).

[13] G. J. de Valcárcel *et al.*, Phys. Rev. A **54**, 1609 (1996).

[14] S. Longhi and A. Geraci, Phys. Rev. A **54**, 4581 (1996).

[15] V. J. Sánchez-Morcillo *et al.*, Phys. Rev. A **56**, 3237 (1997).

[16] G. J. de Valcárcel, Phys. Rev. A **56**, 1542 (1997).